AN X-RAY DOUBLE CRYSTAL SPECTROMETER STUDY OF SINGLY-IONIZED SODIUM-IMPLANTED MAGNESIUM OXIDE

by

RICKY LYNN WORKMAN

B.S., Mississippi State University, 1972

A MASTER'S THESIS

submitted in partial fulfillment of the
requirements for the degree

MASTER OF SCIENCE

Department of Physics

KANSAS STATE UNIVERSITY
Manhattan, Kansas

1974

Approved by:

Major Professor

This is for Mr. and Mrs. C. E. Workman, my mother and father, who cared enough to show me the way, and who, along with my brother Randy, worked so hard and sacrificed so much to give me this opportunity.

TABLE OF CONTENTS

LIST OF FIGURES

INTRODUCTION

In recent years extensive study has been given to the effects of radiation, including neutrons, gamma rays, and heavy and light charged particles, impinging on solids, and numerous papers appear in the literature on the general subject area. In addition to the use of radiation as a probe to better understand solid matter, interest stems from two broad practical applications. First, the desire to utilize more fully ion implantation by the microelectronics industry; and second, the need to understand the changes in properties that result in materials exposed to radiation. Material damage around nuclear reactors has motivated much of the work in this field. It is not surprising, then, that as extensive as the work has been much of it has been confined to studies of semi-conductors, notably silicon and germanium, metals and alloys, fuel element materials, and graphite. Also considerable work has been done on irradiated alkali halides.

A number of techniques can be employed to study lattice damage, each giving a different, but not independent type of information. Some of the physical properties examined are resistivity, electronic behavior, substitution and interstitial lattice modification, crystal structure degradation and especially in the case of construction materials, plasticity, ductility, and tensile strength.

This paper is a study on Magnesium Oxide, MgO, which has been implanted with singly-ionized sodium. The technique chosen is to compare the intensity reflection curves, or rocking curves, of irradiated and unirradiated crystals of MgO on an x-ray double crystal spectrometer.

An examination of the literature reveals only a few papers in which the double crystal spectrometer is used. Thomas, Baldwin, and Dederichs[15] examined the diffuse scattering from neutron irradiated copper crystals using the double crystal technique, and Kishino and Noda[8] have similarly observed bending in irradiated silicon wafers. Petry and Pluchery[14] have studied the rocking curves of neutron irradiated aluminum oxide. Patel, Wagner, and Moss[13] and Bachmann, Baldwin, and Young[1] have used the double crystal spectrometer to study dislocations in silicon and copper, respectively. Rocking curve widths were quoted in these latter two papers, however the samples were not irradiated. Theoretical work to aid in interpreting the curves is similarly scarce, those by Dederichs[6] and by Krivoglaz and Ryaboshapka[9] being the only papers to date. Photoluminescence in irradiated MgO has been studied by Crawford and Dragsdorf[5], but the literature contains no double crystal work done on MgO.

Despite the scarcity of references, the double crystal spectrometer can be an effective tool in this type of work because of its high precision, and the absence of dispersion. An x-ray beam falls on a monochromating crystal whose Bragg reflection is incident on the crystal under study. The second crystal is rotated about the Bragg angle and the reflected intensity detected and plotted as a function of angle. The width of the curve at half maximum, which is only a few arcseconds for perfect crystals, and the area under the curve, the integrated intensity, are indicators of crystal perfection. From the changes in the curves of irradiated and unirradiated portions of the crystal, a qualitative argument as to the nature of the lattice damage will be proposed. A more detailed discussion

of the meaning of the curves will be presented in the theoretical section.

This research also consisted in bringing the apparatus, which had only lately been constructed, to research caliber operation and in demonstrating this by taking diffraction curves of a known nearly perfect crystal. Considerable time was also invested in perfecting a system to measure angles on the order of tenths of seconds of arc. These developments will be discussed along with the results on the MgO sample in the experimental section of this paper.

THEORY

Before turning to the experiment itself, a discussion of the theoretical foundation is necessary and will be presented in two parts. First, the double crystal rocking curve will be examined in order to understand what it means, what factors affect it, and how it is related to single crystal diffraction curves. This will be followed by some considerations of how these curves may change upon irradiation of the crystal, what the changes imply about the crystal, and a brief discussion of MgO. It should be emphasized that the theorectical treatment of radiation damage and x-ray work is quite complicated and is beyond the scope of this paper. Instead, a simple argument and calculation will be presented here, to try to explain some of the experimental observations.

Since an understanding of the rocking curve is all that is desired from the first topic, Darwin's approach is chosen for its simplification over that of Ewald. The two theories give similar results. Further, absorption will be considered negligible. Later, it will be indicated how absorption affects the curve. The single crystal reflection will be developed first, then it will be extended to the double crystal case.

The Single Crystal

Consider a monochromatic beam with wavelength λ and unit amplitude incident at angle Θ on a unit group of atoms forming a set of parallel planes spaced a distance d apart. If there are N atoms per unit volume and F is the structure factor of the unit group of atoms, Darwin showed the amplitude of the reflection coefficient to be,

$$iq = \frac{iNd\lambda}{\sin\theta}\frac{e^2}{mc^2}|F| \qquad (1)$$

In equation (1) e and m are the electronic charge and mass, respectively; and c is the speed of light. The factor i arises from the 90^o phase shift that occurs upon reflection.

Now, with the aid of eq. (1) the intensity of the reflection from the surface of a crystal with planar spacing d can be calculated. The problem is shown in Fig. (1). The planes are indexed by the letter r, r=0 for the surface plane. Let T_r and S_r be the incident and reflected waves, respectively just above the r^{th} plane. If the amplitude ratio S_o/T_o is determined, the ratio of the intensites I/I_o follows. The experiment that one might imagine is to set the crystal at some angle near the Bragg angle and then rotate it through the Bragg angle. The ultimate goal is to know I/I_o as a function of angle.

After some consideration of Fig. (1), one can see that S_r consists of two terms, one from the amount of T_r that is reflected by the plane r, which is just $T_r(iq)$, and the other from that part of S_{r+1} transmitted through the plane r. This is given by $S_{r+1}(1+iq_o)(1-h)e^{-i\phi}$, where $(1+iq_o)$ is the transmission coefficient, (1-h) is an absorption term, and q_o is given by,

$$q_o = \frac{Nd\lambda}{\sin\theta}\frac{e^2}{mc^2}f(0)$$

The phase $e^{-i\phi}$ is necessary because S_{r+1} is the amplitude just above the r+1 plane, so the wave travels a distance $d\sin\theta$ to arrive at the plane r. It thus requires a phase term and ϕ is given by,

Fig. 1: Atomic planes as related to the Darwin approach to calculating the reflected intensity.

FIGURE 1

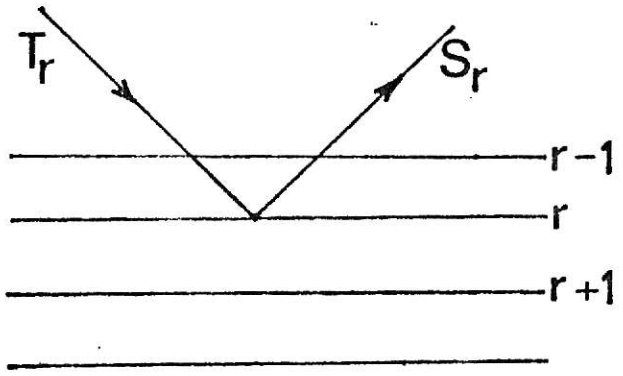

$$\phi = \frac{2\pi d}{\lambda} \sin \Theta.$$

Now S_r can be written as,

$$S_r = T_r(iq) + (1-h+iq_o)S_{r+1}e^{-i\phi} \tag{2}$$

where second order terms in the product $(1-h)(1+iq_o)$ have been dropped.

Similarly, T_{r+1} has two terms, the first from the part of T_r transmitted through plane r, which is T_r times the transmission coefficient including the absorption. The second term is the part of S_{r+1} reflected from the $r^{\underline{th}}$ plane, which is the product of S_{r+1} and the reflection coefficient iq. The phase here will be $e^{-2i\phi}$ since the path $2d\sin\Theta$ is traversed twice. Thus,

$$T_{r+1} = T_r(1-h-iq_o)e^{-i\phi} + S_{r+1}(iq)e^{-2i\phi}. \tag{3}$$

Eqs. (2) and (3) are the difference equations from which Darwin obtained the amplitude ratio S_o/T_o to be

$$S_o/T_o = \frac{iq}{h+iv \pm (q^2+h+iv)^{\frac{1}{2}}} \tag{4}$$

where v is related to a small difference in angle given by

$$v = \frac{2\ d\ \cos\ \Theta(\Theta-\Theta_o)}{\lambda}$$

and Θ_o is given by

$$m\lambda = 2d\sin\ \Theta_o[1 - (1-n)/\sin^2\Theta]$$

which is the Bragg law, corrected for the index of refraction, n, of the crystal.

Eq. (4) can be made more tractable and the information more easily obtained if the absorption is negligible, i.e. h = 0. This along with the following definitions.

$$E = \frac{v\lambda}{2\pi d\cos\theta} = \theta - \theta_o \tag{5}$$

and

$$s = \frac{q}{2\pi d\cos\theta} \tag{5a}$$

gives

$$S_o/T_o = \frac{1}{E/s \pm [(E/s)^2 - 1]^{\frac{1}{2}}} \tag{6}$$

The choice of sign is made to satisfy the condition $S_o/T_o \leq 1$.

Since it is the intensity ratio $I/I_o = R(E)$, i.e. the reflection coefficient that is of interest, the modulus of eq. (6) must be taken and squared. This is done in two parts and yields,

$$R_I(E) = \frac{1}{(E/s)^2 + 1 - (E/s)^2} = 1 \qquad \text{for } (E/s)^2 < 1 \tag{7}$$

$$R_0(E) = \frac{1}{2(E/s)^2 \pm 2(E/s)[(E/s)^2 - 1]^{\frac{1}{2}} - 1} \quad \text{for } (E/s)^2 > 1$$

A plot of eqs. (7) is shown in Fig. (2), and is the reflection coefficient as a function of angle for a perfect crystal with no absorption. There is total reflection over an angular width of 2s. Experimentally, the width at half maximum, w_s, is the quantity of interest which will be slightly more than 2s due to the wings, and it is in fact 2.12s, where

Fig. 2: Upper curve shows the perfect single crystal rocking curve with negligible absorption; lower curve is the result when absorption is included. (See Reference 16).

FIGURE 2

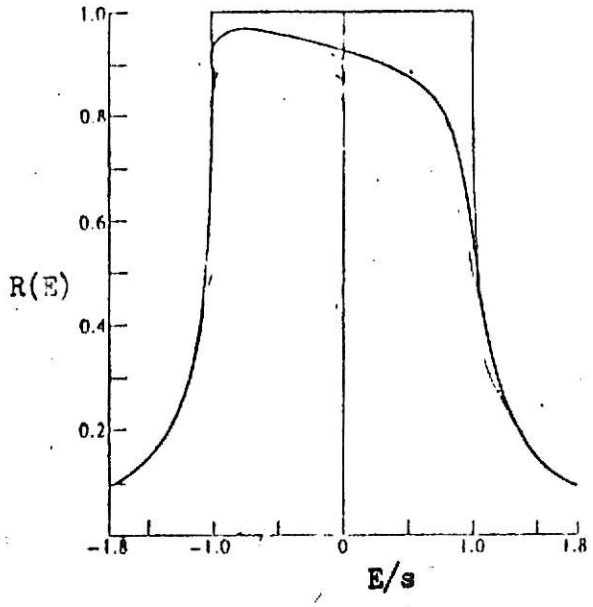

$$s = \frac{e^2 N \lambda^2}{mc^2 \pi \sin 2\theta} |F| \qquad (8)$$

No mention has been made about the polarization of the x-ray beam, which affects the width and shape of the R(E) versus E curve. If the atoms scatter as a point and the beam is polarized with electric field vector perpendicular to the plane of incidence, the curve is as shown, but for real atoms the range of total reflection contracts, and in fact occurs on only the positive side of E = 0. If the electric field vector is polarized parallel to the plane of incidence, the range of total reflection also contracts. For unpolarized radiation, there is a sum of these two intensities, and hence the result also is contracted, and the corners are rounded. For an unpolarized beam eq. (8) becomes

$$s = \frac{e^2 N \lambda^2}{mc^2 \pi \sin 2\theta} |F| \ (1 + \cos 2\theta)/2 \qquad (9)$$

If one substitutes the proper quantities into eq. (9) for calcite a value of 7.61 arcseconds is obtained for w_s.

When absorption is included, the curve of Fig. (2) becomes asymmetric and looks like the lower curve in Fig. (2).

Another experimental quantity of interest is the integrated intensity, which is the area under the reflection curve. This can be calculated by integrating eqs. (7) over infinite limits which gives,

$$I_{sc} = \frac{8}{3} s = \frac{8}{3\pi} \frac{e^2}{mc^2} \frac{N^2 \lambda^2}{\sin 2\theta} |F| \ (1 + \cos 2\theta)/2 \qquad (10)$$

If the crystal under study is not perfect, it can be thought of as being

made up of mosaic blocks with slightly different orientations. Then, as one block is satisfying the Bragg condition, another block will be nearly doing so. This will cause the reflection curve to broaden and the intensity peak to diminish. The integrated intensity will increase. In the case of the ideally imperfect crystal, the integrated intensity has a different form,

$$I_{sc}^{imp} = \frac{N^2 \lambda^2}{2\mu_\ell} |F|^2 \left(\frac{e^2}{mc^2}\right)^2 \left(\frac{1 + \cos^2 2\Theta}{2\sin 2\Theta}\right) \qquad (10a)$$

where μ_ℓ is the linear absorption coefficient.

The requirement made above for a monochromatic beam parallel to within a few seconds of arc is a very stringent one experimentally. The fact that there is no monochromatic x-ray source, not only puts the value of the above treatment in question, but also seems to imply that a perfect crystal diffraction could not be observed. The effect of dispersion would wash out a curve only a few arcseconds wide.

The Double Crystal Spectrometer

By introducing a monochromating crystal between the source and the crystal under study, these conditions can be very nearly satisfied. This is the principle of the double crystal spectrometer, see Fig. (3). If the first crystal, crystal A, is positioned so that it satisfies the Bragg condition, the reflection from crystal A will be nearly monochromatic, having a wavelength spread less than that of a typical x-ray characteristic line. Now, one may imagine doing an experiment similar to that described earlier, by putting the second crystal, crystal B, in this reflected beam

Fig. 3: (a) The parallel, or (n,-n) orientation of the double crystal spectrometer.

(b) The anti-parallel or (n,n) orientation.

FIGURE 3

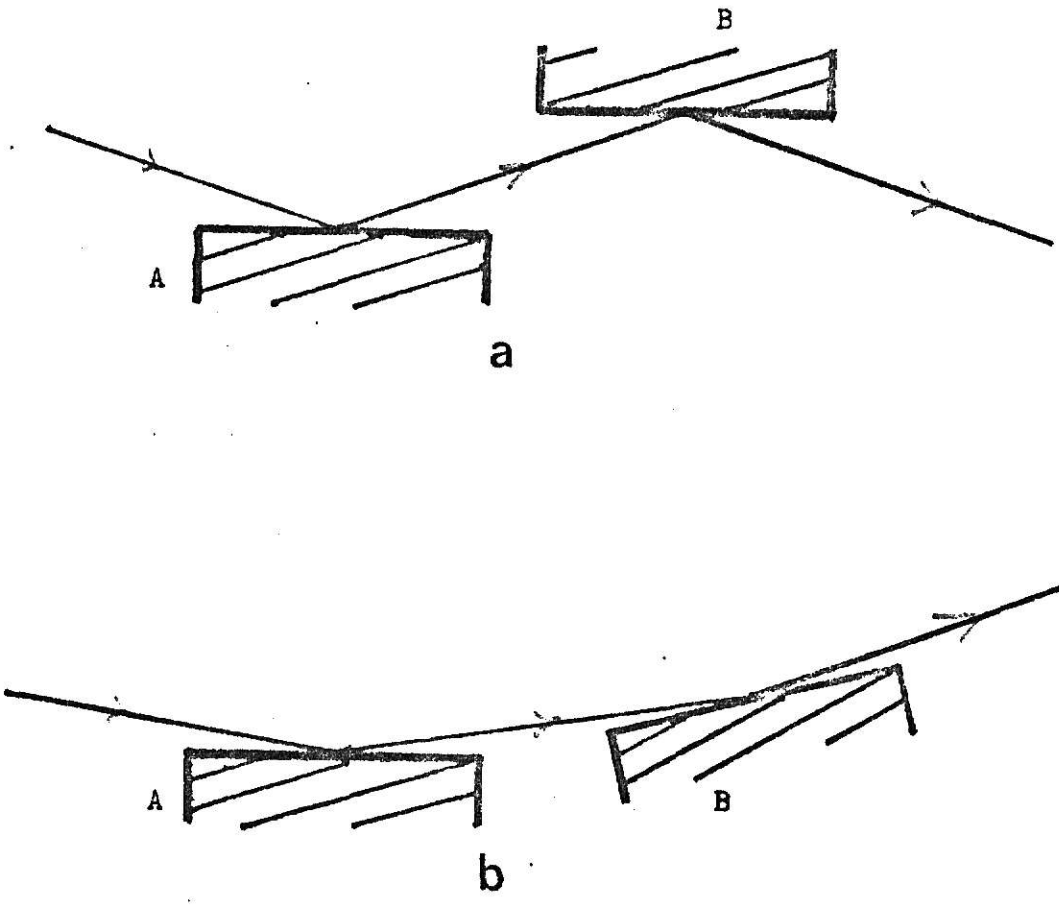

and rotating it, through an angle X about the Bragg angle. Again the reflection coefficient as a function of angle is the expression sought, and the width and integrated intensity are the quantities of interest. The following treatment is a synthesis of that given by James[10] and Compton and Allison[4].

Let n_A and n_B be the orders of interference for crystal A and crystal B, respectively. There are two possible orientations; the parallel or $(n_A,-n_B)$ shown in fig. (3a) and the anti-parallel or (n_A,n_B) in fig. (3b). The parallel configuration was used entirely in this experiment, and is the only one that will be considered here.

Now, suppose the incident beam has horizontal divergence Y, that the Bragg angle for both crystals for the wavelength λ_o is Θ_o, and the glancing angles for λ_o and some other wavelength λ be Θ and $\Theta + d\Theta$, respectively. Note,

$$d\Theta_A = (\lambda-\lambda_o) \frac{\partial\Theta_{n_A}}{\partial\lambda}$$

and

$$d\Theta_B = (\lambda-\lambda_o) \frac{\partial\Theta_{n_B}}{\partial\lambda} .$$

Further, let the reflection coefficient of crystal A be $R_A(Y-d\Theta_A)$ and of crystal B be $R_B(Y-d\Theta_B-X)$, when B is set at the angle X with respect to the parallel position. The functional form of the reflection coefficients R_A and R_B could be that of eqs. (7) if the crystals A and B are perfect. In any case, the important thing to notice is that the reflection coefficients have appreciable value only when their arguments are very nearly zero. The total power reflected by crystal B set at angle X is

$$P(X) = \int_{\lambda_{min}}^{\lambda_{max}} J(\lambda-\lambda_o)d\lambda \int_{Y_{min}}^{Y_{max}} G(Y)\, R_A(Y-d\theta)R_B(Y-d\theta-X)dY$$

where G(Y) is a geometrical factor depending on the distribution of intensity in the incident beam, and $J(\lambda-\lambda_o)$ is proportional to the intensity included in wavelengths λ to $\lambda + d\lambda$. The reflection coefficients are taken to be independent of wavelength, which is very nearly true over the small region of wavelengths in an x-ray beam, such as the characteristics Kα line since the reflection coefficients have a significant value only when their arguments are nearly zero. Then for R_A to have appreciable value, $Y \tilde{=} d\theta$, and this implies in R_B that X is on the order of the rotation angle in the single crystal. Hence, the width measured with the double crystal unit will be on the order of the width of the single crystal. The double crystal curve for a perfect crystal should be on the order of a few seconds of arc. In addition, the requirement that $\tilde{Y} = d\theta$ says that the first crystal is spreading the beam into monochromatic, parallel beams. The important fact is that, not only will the width of the double crystal curve be about that of the single crystal, but that the double crystal spectrometer can resolve this because there is no dispersion in the parallel position. This can be readily shown by setting the arguments of the reflection coefficients equal to zero.

$$Y - d\theta_A = Y - (\lambda-\lambda_o)\frac{\partial\theta_{n_A}}{\partial\lambda} = 0$$

$$Y - d\theta_B - X = Y - X - (\lambda-\lambda_o)\frac{\partial\theta_{n_B}}{\partial\lambda} = 0$$

Eliminating Y and re-arranging gives,

$$X = (\lambda-\lambda_o)\left(\frac{\partial\Theta_{n_A}}{\partial\lambda} - \frac{\partial\Theta_{n_B}}{\partial\lambda}\right).$$

Let D be the quantity in brackets, then,

$$X = (\lambda-\lambda_o)D.$$

The dispersion is $dX/d\lambda$ which is just D by the above. Using the Bragg law and carrying out the differentiations, D can be rewritten as,

$$D = \frac{n_A}{2d\cos\Theta_{n_A}} - \frac{n_B}{2d\cos\Theta_{n_B}}$$

If the crystals are the same, D = 0 and there is no dispersion.

If crystals A and B are the same, which is the case of experimental interest, the equation for the reflected power can be rewritten with R_A and R_B having the same functional form and the subscripts can be dropped. Further, since the values of Y over which the R's have appreciable value is small, the limits on the integral can be extended to plus and minus infinity, and G(Y) can be taken to be constant over the narrow range of Y used here. The expression for the power can be written,

$$P(X) = K\int_{-\infty}^{+\infty} R(Y-d\Theta)R(Y-X-d\Theta)dY \qquad (11)$$

where the integral over the wavelength is included in the constant K. To obtain the reflection coefficient for the second crystal, crystal B, eq. (11) must be divided by a normalizing factor given by,

$$\int_{-\infty}^{+\infty} G(Y)\, R_A(Y - d\Theta)dY \int_{\lambda_{min}}^{\lambda_{max}} J(\lambda-\lambda_o)\, d\lambda$$

which is the integrated reflection from crystal A. But since this is also the integrated reflection for B since $R_A=R_B$, it is constant and the expression for the reflection coefficient of crystal B, $R_2(X)$, is,

$$R_2(X) = K' \int_{-\infty}^{+\infty} R(Y-d\Theta)R(Y-X-d\Theta)dY \qquad (12)$$

Eq. (12) says that the reflection coefficient of the second crystal at angle X from the parallel position is the convolution of the reflection coefficients of the two crystals. Further, a plot of eq. (12) will not have the flat top as shown for the Darwin single crystal in Fig. (2), but will have a maximum at X=0. If $R_2(0)$ is calculated the value 4/5 is obtained rather than one, so total reflection cannot be observed with this device. The curve $R_2(X)$ is symmetric no matter how asymmetric are the R's. One might ask if the individual reflection coefficients could be determined from $R_2(X)$, but it has been shown that this cannot be done unless it is assumed that the individual R's are symmetric, which is not a good assumption. The best that can be done is to guess a form for the R's and calculate $R_2(X)$ and compare the result with the observation. Fig. (4) shows this process. Note that when a Darwin shape is chosen for the individual R's, Fig. (4), the agreement with experiment is poorer than when absorption is included Fig. (4).

Depending upon the form chosen for the individual R's in the convolution, the width of the double crystal curve, w_D, can be calculated from

Fig. 4: (a) A calculated single crystal rocking curve for calcite.
(b) An experimentally observed double crystal rocking curve compared to that calculated double crystal curve using the function of (a) in the convolution. The dotted and solid curves refer to the experimental and theoretical findings, respectively. (See Reference 4)

THIS BOOK CONTAINS NUMEROUS PAGES WITH DIAGRAMS THAT ARE CROOKED COMPARED TO THE REST OF THE INFORMATION ON THE PAGE.

THIS IS AS RECEIVED FROM CUSTOMER.

ILLEGIBLE DOCUMENT

THE FOLLOWING DOCUMENT(S) IS OF POOR LEGIBILITY IN THE ORIGINAL

THIS IS THE BEST COPY AVAILABLE

FIGURE 4

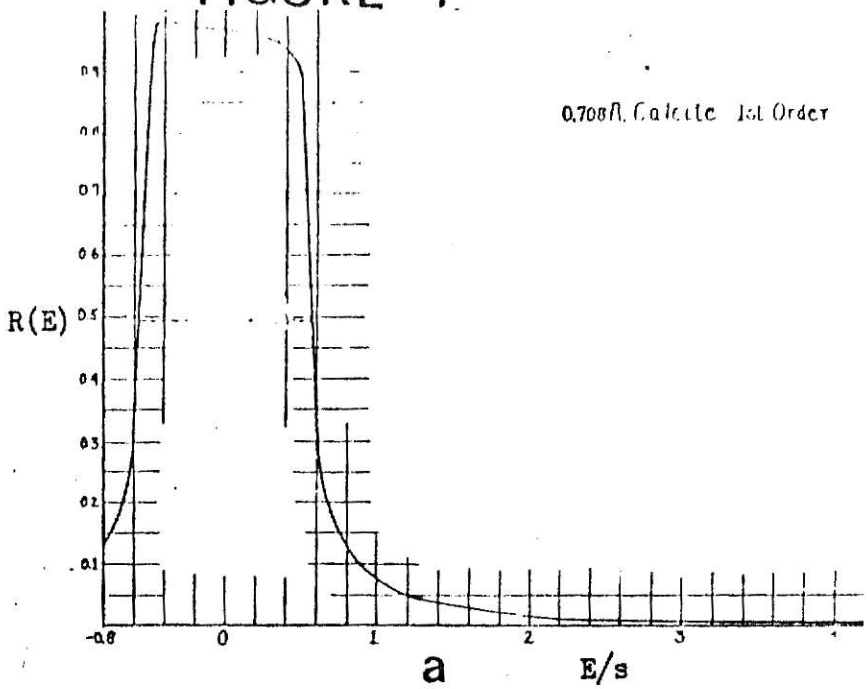
0.708Å. Calcite 1st Order
R(E)
-0.8
0
1
2
3
a
E/s

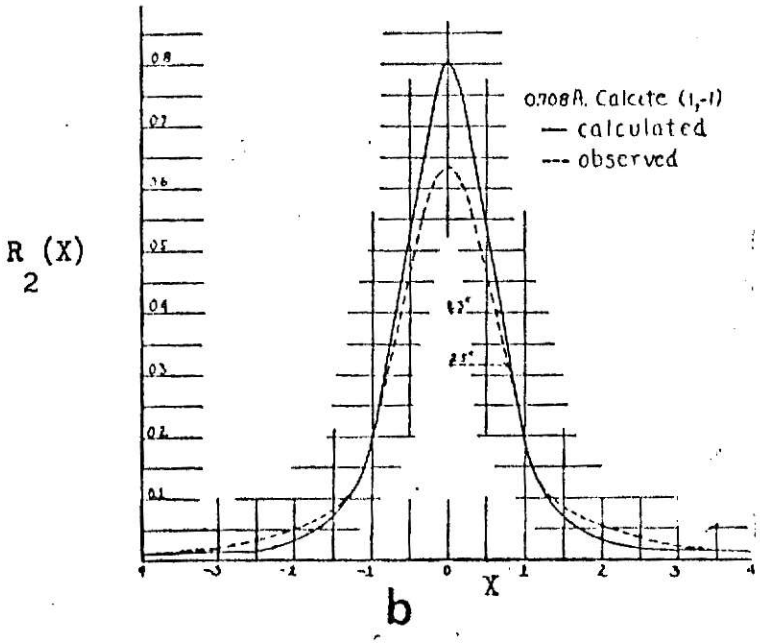
0.708Å. Calcite (1,-1)
— calculated
--- observed
R (X)
2
X
b

Fig. 4 (cont.): (c) Another calculated single crystal rocking curve for calcite, this time including absorption and polarization.
(d) When the function of (c) is used in the convolution, a much better fit is obtained to the experimental double crystal rocking curve. (See Reference 4).

FIGURE 4 (cont.)

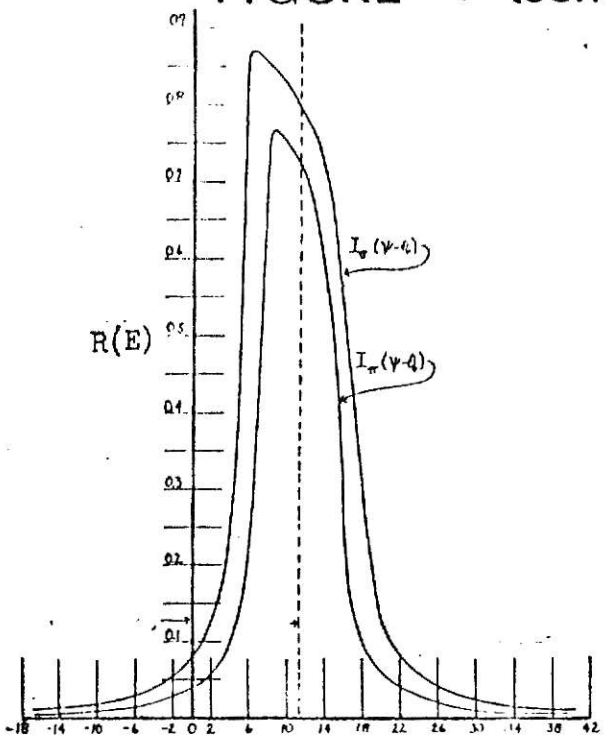

c

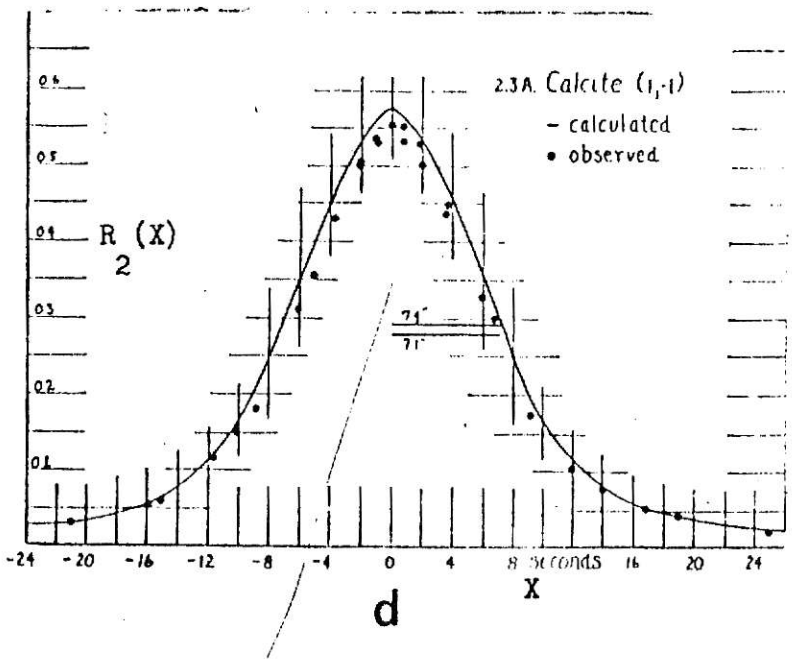

d

the width of the single crystal curve, w_s. For example, if the individual R's are chosen to have the flat top shape of a Darwin perfect crystal, $w_D=1.32w_s$, but if Gaussian shapes are chosen, $w_D=1.414w_s$.[10]

To include the effect of polarization in eq. (12), the equation must be written in terms of an $R_\sigma(Y)$, $R_\sigma(Y-X)$, $R_\pi(Y)$, and $R_\pi(Y-X)$.

$$R_2(X) = \int \frac{\{R_\sigma(Y)R_\sigma(Y-X) + R_\pi(Y)\, R_\pi(Y-X)\}dY}{\int\left(R_\sigma(Y) + R_\pi(Y)\right)dY} \qquad (13)$$

The integrated intensity can be calculated from eq. (13) by integration, which in general is quite hard. However, if R_σ and R_π have Darwin shapes, the integrated intensity is,

$$I_{DC} = \frac{2(1 + \cos^2 2\Theta)\, I_{SC}}{(1 + \cos 2\Theta)} \qquad (14)$$

Thus, it has been shown that the double crystal spectrometer does give a monchromatic, parallel beam, with zero dispersion when the two crystals are identical and in the parallel position; that is, the reflection coefficient's shape and width are independent of the wavelength, which allows the narrow widths of perfect crystals to be observable. Further, the reflection curve will be of the same order of width as the single crystal, the exact relationship depending on what R(Y) is put into the convolution.

Ion Implantation

Now that the meaning of the rocking curve has been established, one may ask what changes to expect upon irradiation. The discussion will be

restricted to the case where ion implantation is the type of radiation used, as this was the case in the experiment. When a beam of heavy charged particles strikes the crystal, energy losses first occur by electronic processes, exitation and ionization. After losing enough energy through these processes, nuclear collisions are the dominant means of energy loss. Fig. (5) is a plot of the number of ions deposited versus the depth in the crystal. The constant portion represents energy loss by electronic processes, and hence, few ions are deposited in this region. The peak represents that region where the incident particles are slowed by collisions and come to rest. These collisions with the ions in the lattice produce vacancy-interstitial pairs or Frenkel pairs. Thus the incident ions come to rest at interstitial sites and the lattice atoms knocked from their lattice sites also become interstitials. The depth, R_p, at which most of the ions are deposited is called the projected range, and ΔR_p is the deviation from the projected range. Half of the ions are deposited in a region of $\pm\Delta R_p$ around R_p. Linhard, Scharff, Schiott[11] have worked out a theory to calculate R_p and ΔR_p, and the values for some implants and host crystals are tabulated for given energies.

A simple picture of the irradiated crystal is shown in Fig. (6). As mentioned above the implant will produce many interstitials and vacancies in a region of depth R_p, shown as region I in Fig. (6). One expects this region to expand due to the presence of the interstitials, and if x-rays are incident on planes lying in the expanded region, a Bragg peak should appear at a lower angle than the original peak, due to the increased planar spacing. Region II in Fig. (6) is just below the implanted volume, and it should have the same planar spacing as an unimplanted sample. Thus x-rays

Fig. 5: The number of incident ions deposited as a function of the depth in the crystal. The constant region represents energy loss by electronic processes, while the peak results from collisions. (See Reference 11)

FIGURE 5

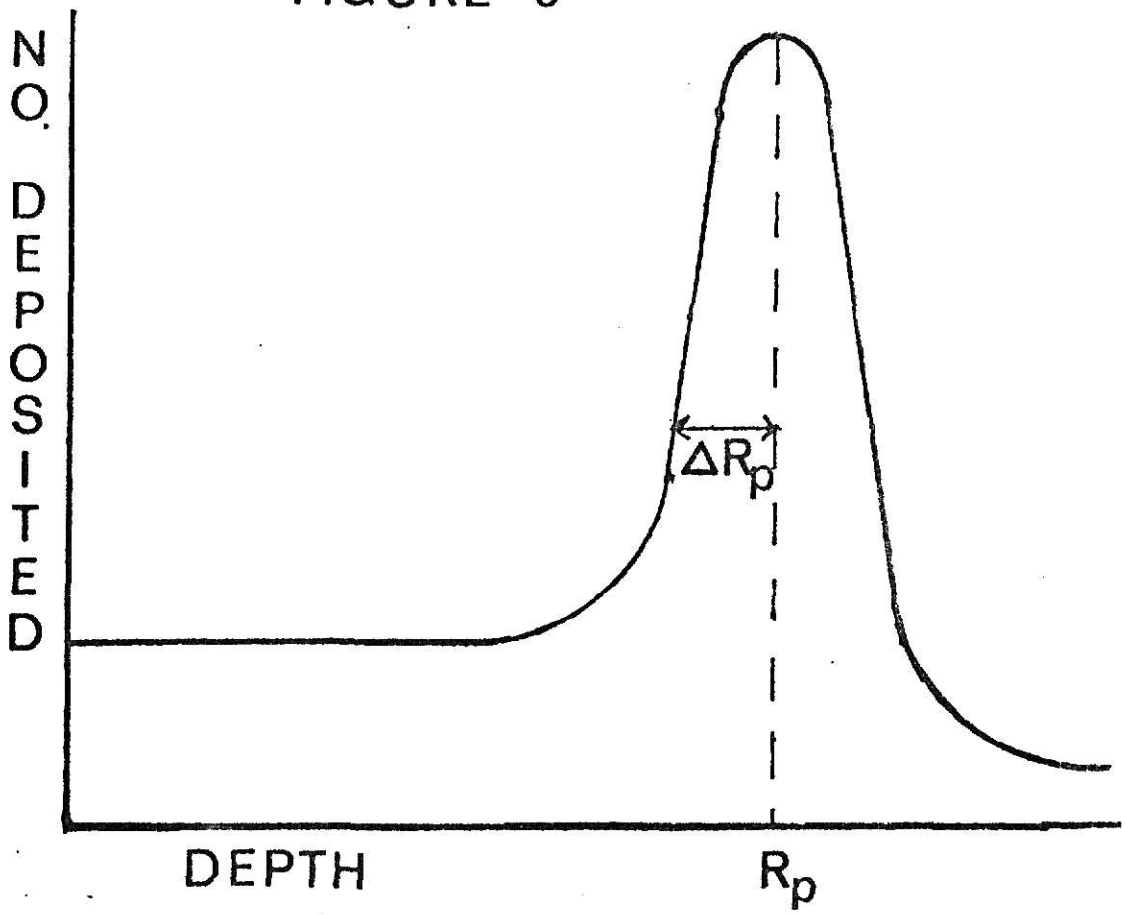

Fig. 6: The three basically different regions from which x-rays can be diffracted in the implanted crystal.

FIGURE 6

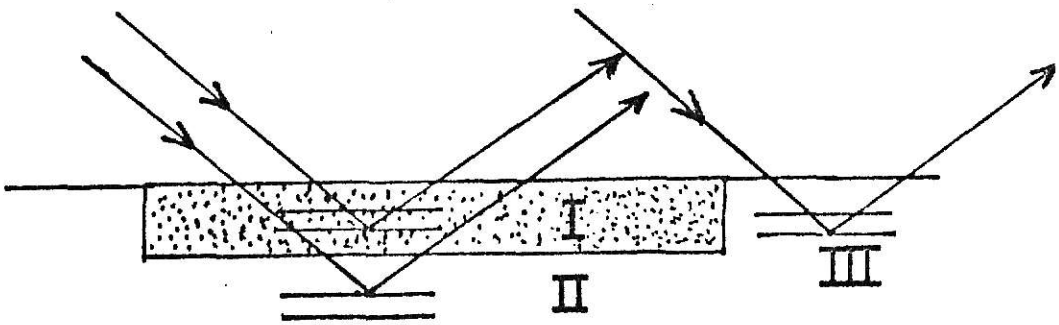

incident on planes in region II should give the same Bragg peak as observed in the unimplanted sample. However, one may expect this peak to be of lower peak intensity since a smaller volume is contributing to this reflection. The peak may have a wider full width at half maximum w_D, due to some strain near the implanted layer. This lattice strain will also act to reduce the peak intensity. A similar result is to be expected for diffraction by planes in region III. The intensity may be higher for region III since the x-rays do not have to penetrate the implant. If there is some damage to the sides of the implanted layer, the curve taken for region III will also be broader than that of an unimplanted sample. It should be noted that diffraction from region II presumes that the implanted layer is not greater than the penetration depth of the x-rays. This is usually the case for ion implantations, and certainly is true under the conditions of this experiment. Thus one expects the rocking curve taken in the implanted area to have two peaks; one at the same angle as observed for the unimplanted crystal which will be somewhat lower and broader, and a second peak at a lower angle due to the increased planar spacing of the implanted layer.

As a simple theoretical treatment, the following calculation for the angular separation of the two peaks is presented. The results of this calculation can then be compared to the experimental results. Consider a cubic crystal, such as MgO, with a unit cell of length a on a side with planar spacing d=a/2. Let a' be the length of the side of the unit cell in the expanded lattice and $\Delta a = a' - a$. The angular shift $\Delta\theta$, may be expressed in terms of a and Δa by differentiating Bragg's law,

$$\Delta\Theta = \frac{-\Delta d}{d} \tan \Theta_B .$$

But $\Delta d/d = \Delta a/a$ and,

$$\Delta\Theta = -(\Delta a/a)\tan \Theta_B \qquad (15)$$

In order to calculate $\Delta\Theta$ in eq. (15), a method of calculating a' must be found. One can do this easily if the volume of the expanded unit cell, V_c', is known. Suppose that the host crystal has p ions per unit volume before the implant and p' afterwards. The number per unit volume will be called the packing rate. Since most of the ions come to rest in the region $\pm \Delta R_p$. The volume of the implant V_I will be the product of the area of the crystal irradiated and $2\Delta R_p$ for a particular ion of given energy. The number of host crystal molecules in V_I is $N = pV_I$, and the number of unit cells in V_I is N_c.

Now the implantation adds n ions in the volume V_I, and as discussed earlier, this causes V_I to expand. The expanded volume can be calculated by dividing the number of particles n+N by the packing rate after implantation, p'. One would expect p' to differ from p due to two effects. First, if significant vacancies are produced, this would act to make p' less than p. Second, p' should differ from p by a factor containing the packing rate of the ions introduced. Depending on the size of the implanted ion compared to the size of the hosts, this could make p' smaller or larger than p. If the ion is larger, then p' will be smaller than p. The quantity p' can be expressed as the sum of three terms, the value of the host p, a term to take into account the packing rate of the interstitial ions, p_i, and a third term, p_v, to account for the vacancies. p_v will tend to make p' less

than p. A vacancy will result in an increased equilibrium separation due to coulombic repulsion, and there will be increased volume. Thus vacancy production will tend to decrease p and p_v has a minus sign.

The expanded volume then is

$$V' = \frac{n+N}{p'} = \frac{n + N}{p + p_i - p_v} . \tag{16}$$

However, to get the new cube length, a', the volume of the expanded unit cell is needed. The implant does not change the number of unit cells so dividing eq. (16) by N_c yields,

$$V'_c = \frac{n + N}{p'N_c} \tag{17}$$

and

$$a' = (n+N/p'N_c)^{1/3} \tag{18}$$

By substituting eq. (18) into eq. (15), the angular shift is,

$$\Delta\Theta = [(n+N/p'a^3N_c)^{1/3} - 1] \tan \Theta_B \tag{19}$$

The angular shift for Na^+ ions implanted in MgO at 90 kev, the conditions of the experiment, could be calculated easily with eq. (19) if p' is known. Unfortunately, the details of how the Na^+ ions pack in the MgO is not known and thus no value for p_i or p_v is available. However, if it is assumed that p' = p, that is $p_v = p_i$, a value of $\Delta\Theta$ can be obtained. Since each vacancy results in an interstitial, this is not an unreasonable assumption to make, at least in a first approximation. A value of the angular shift can now be calculated using the following data;

a_{MgO}=4.213 Å, θ_B for (200) of MgO = 21.47°, 4 MgO molecules per unit cell. Then

$$p = \frac{8 \text{ ions/unit cell}}{(4.213)^3 \times 10^{-24}} = 1.0698 \times 10^{23} \text{ ions/cc}$$

The area is defined by a set of slits placed in the accelerator beam which were (0.68cm.) X (0.66cm.). The effective range of Na^+ ions in MgO has been calculated according to the program of Johnson and Gibbons[7] by Crawford and Dragsdorf[5] to be 929 Å at 90 kev. Thus,

$$V_I = (.68)(.66)(4.58 \times 10^{-6})cc = 2.0555 \times 10^{-6}cc.$$

$$N_c = V_I/(4.213)^3 \times 10^{-24} = 2.748 \times 10^{16}$$

and,

$$N = pV_I = 2.199 \times 10^{17}$$

There are 2.5×10^{15} Na^+ ions added, and eq. (19) gives,

$$\Delta\theta = \{[(2.5 \times 10^{15} + 2.199 \times 10^{17})/2.199 \times 10^{17}]^{1/3} - 1\}(.393)$$

$$= 306 \text{ arc seconds.}$$

This is the value to be compared with the observation. The agreement will depend largely on how valid the assumptions made in the calculation are for the experiment. If eq. (19) is rewritten with p' replaced by $p + p_{eff}$, p_{eff} can be calculated from the experimental data, and thus provide a means of examining the assumptions quantitatively. It should be noted that it was a matter of choice as to how to correct p for the vacancies and interstitials. Instead, of treating it as an addition, p could have been modified by a multiplicative factor. Which method is best will have

to be determined by the agreement achieved with this and other experiments. The above is only a starting point. To determine how well it will explain the results, the experimental work must now be considered.

EXPERIMENT

Development of the Apparatus

The double crystal spectrometer used in this experiment was constructed at Kansas State University to accompany a General Electric XRD-6 X-Ray Diffractometer. The XRD-6 consists of an x-ray tube power supply, and a detection system with a pulse height selector and amplifier, a scaler counting unit and a counting rate meter. A printer is attached which records the x-ray counts over a preset period of time.

Copper Kα radiation was used throughout this experiment with the tube operated at 30 kilovolts with a filament current of 10 milliamps. From the port on the x-ray tube, the beam traverses two vertical collimating slits, before being incident on the first crystal.

The spectrometer itself is shown in Fig. (7). It consists of two turntables, adjustable through 360° by gears which were cut to give tenth of a second of arc increments. The turntables are flush with a massive steel housing which conceals the gears. There are also gear adjustments to rotate the entire assembly about the axis of the first turntable and for positioning the x-ray counter. The x-ray counter used in this experiment was a General Electric SPG 10 proportional counter operated throughout the experiment at 1500 volts. This value was selected from a plot of counts versus power supply voltage to determine the region in which the counts were most nearly constant with change of power supply voltage. The two crystal mounts that attach to the turntables each has an adjustment screw to allow movement parallel and perpendicular to the beam. In addition, the second crystal mount has a screw adjustment for tilt with respect to the beam.

Fig. 7: Top view of the apparatus as used in the experiment with MgO.

FIGURE 7

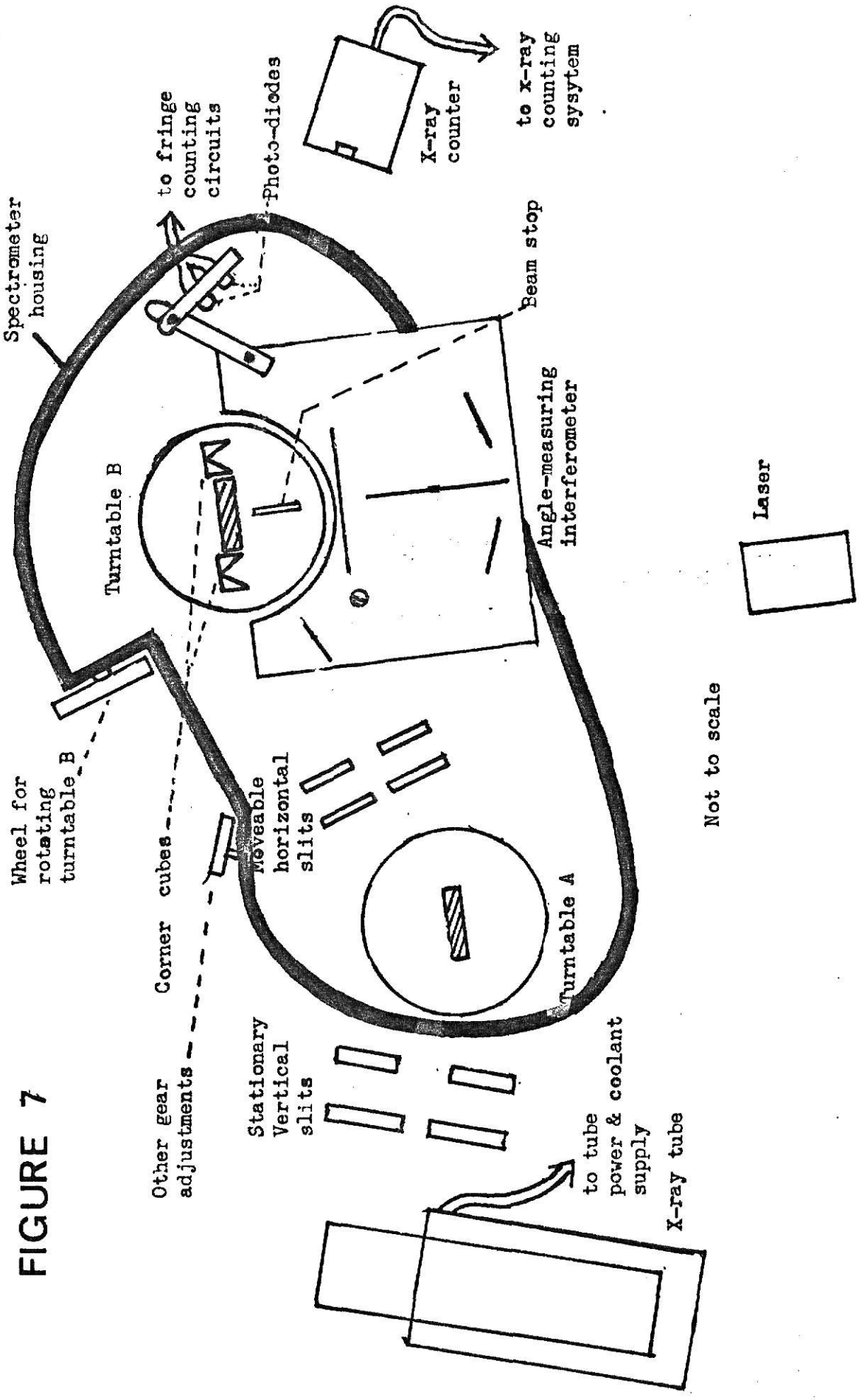
Spectrometer housing
to fringe counting circuits
Photo-diodes
X-ray counter
to x-ray counting sysytem
Beam stop
Turntable B
Angle-measuring interferometer
Laser
Wheel for rotating turntable B
Corner cubes
Moveable horizontal slits
Other gear adjustments
Stationary Vertical slits
Turntable A
to tube power & coolant supply
X-ray tube
Not to scale

As was discussed in the theoretical section, one expects to measure angles to an accuracy of a fraction of a second. Although the gears were designed to provide this, it was quickly found that the slightest imperfection in the gears, and the backlash in the gear train prevented this high precision and another means of measuring angle was required.

To do this an angle measuring interferometer similar in design to that used by Marzolf[12] was constructed. The one used here differs in the use of a Metrologic Model 360 helium-neon laser as a light source and a matched pair of Motorola MDR 310 photo-diodes as detectors. Also an adjustment was devised to allow movement of the photo-diodes with respect to the fringe pattern. The incident laser beam is split by a half-silvered mirror, the two beams then being reflected to a pair of corner cubes mounted on either side of the axis of the second turntable by another set of mirrors. The corner cubes are mounted on a monel metal plate, which is very insensitive to thermal expansion. The inferometer was securely mounted to the housing to insure its stability. The corner cubes consist of a piece of glass that had been cut to form the corner of a cube, and they have the property of reflecting an incident beam back along a path that is parallel to the incident beam. In the design used here the reflected beam from the corner cube, strikes another mirror, returns through the corner cube and back exactly along its original path. The two beams are then brought together at the photo-diodes. Since no beam expander was used on the laser, the interference was only the size of the laser spot, and needed to be enlarged to be spaced properly for the photo-diodes. Two steps were taken to accomplish this. First, the laser was placed across the room so that the

divergence of the beam increased the spot size to about ½ inch, and second, a short focal length cylindrical lens was placed in front of the photo-diodes so that the pattern was spread horizontally, but not vertically. This made the fringes the correct size and spacing.

As the turntable is rotated, the path difference changes, causing the order of interference to change and the fringes to move. As the fringes go by, they are detected by the photo-diodes, which produce a current proportional to the light intensity. The current goes through a gain resistor, and the voltage drop across it is the input to an operational amplifier-type Schmitt trigger circuit. There is a trigger circuit for each of the photo-diodes. The output from the Schmitt trigger is fed to an up-down counter utilizing TTL logic and LED display. In order for the counter to discern up and down counts, the signals from the two channels of the Schmitt trigger must arrive 90° out of phase.

Since much of the time spent on this project was used getting this angle measuring system functioning properly, a brief description of this is in order here. The first difficulty was that of laser intensity. There must be at least 40 millivolts at the input to the Schmitt trigger. Initially the gain resistor was a thousand ohm potientiometer and the current produced by the laser light on the photo-diodes gave a voltage drop of only a few millivolts. A ten thousand ohm resistor was added to the circuit bringing this value to about 50 millivolts. The addition of this large resistor seemed to have an adverse affect on the stability of the circuit, making the other adjustments for switching level and hysteresis very delicate. Finally, a more intense laser was acquired, the other one having lost much of its output, and the ten thousand ohm resistors were replaced by one

thousand ohm resistors. A voltage input of around 70 millivolts was then produced. This seemed to improve the stability problem considerably. When the amplifiers in the Schmitt circuit are switching properly, the fringes must be placed correctly with respect to the photo-diodes to give the necessary 90° phase difference. This is most easily done by moving the diodes slightly in the fringer pattern while observing the input signals of the two channels on an oscilloscope. The photo-diodes are moved until a circle is seen. Then the counter should be working properly. Initially, although these steps were followed, the counter did not work. The problem was traced eventually to a faulty transistor at the Schmitt output and a defective integrated circuit in the counter logic.

The use of this interferometer required some modifications to the mount for the second crystal. The interferometer itself had to be attached to the housing, and the Bragg angle for the second crystal can be such that the corner cubes are at a very skewed angle with respect to the interferometer. The extreme example is in the anti-parallel case, in which the corner cube back would face the interferometer, requiring the interferometer to be moved, which was very inconvenient. To remedy this, the second crystal mount was redesigned to be moveable through 360° so large changes in angle could be made by rotating the crystal mount with the turntable being stationary.

Once the interferometer and counting system were functioning properly, it remained to be calibrated. Of several proposed ways of doing this, the method chosen was to direct a light beam from a slide projector through a very narrow slit onto a mirror fixed on the second crystal mount. This light beam was reflected from the mirror to a set of slits placed in front of the objective of a measuring microscope and securely fastened to it.

The turntable was rotated through a small angle which moved the reflected light beam. The slit and microscope assembly was moved until the slit was centered in the reflected beam and the micrometer reading and fringe count noted. This procedure was followed over a range of 14 minutes in half minute steps. The micrometer movement was the arc length, the mirror to microscope slit distance was the radius allowing the angle to be calculated. Then a plot of angular increment versus the fringe count was made. Fig. (8) shows a least squares fit to the data, from which the slope gives the fringe count to angle conversion to be 1.877 fringes/arc sec. The correlation factor calculated in the fit was 0.99996. A probable error analysis was performed on the data and the uncertainty of the conversion factor was found to be $\pm$ 0.003.

With the angle measuring system calibrated, it was desired to check the linearity of the x-ray counting system. This was done by placing sheets of one mil. thick aluminum foil in front of the counter aperture and a taking a count over a ten second period for each thickness. The pulse height selector and amplifier had been set properly prior to this and were never altered throughout the experiment. Using the absorption equation

$$\frac{I}{I_o} = e^{-\mu_\ell n t_o}$$

where μ_ℓ is the linear absorption coefficient, I_o is the intensity detected with no absorbers, n is the number of aluminum sheets, and t_o is the thickness of one aluminum sheet, a plot of $\ln(I_o/I)$ versus n was made. This should yield a straight line, with a slope equal to the linear absorption coefficient of aluminum which is .33cm^{-1}. The results of data taken over

Fig. 8: Calibration curve for the angle measuring interferometer. The slope, 1.877, is the conversion factor from fringes to angle in seconds. The least squares fit revealed a confidence of 0.99996, and a probable error of $\pm$ 0.003.

FIGURE 8

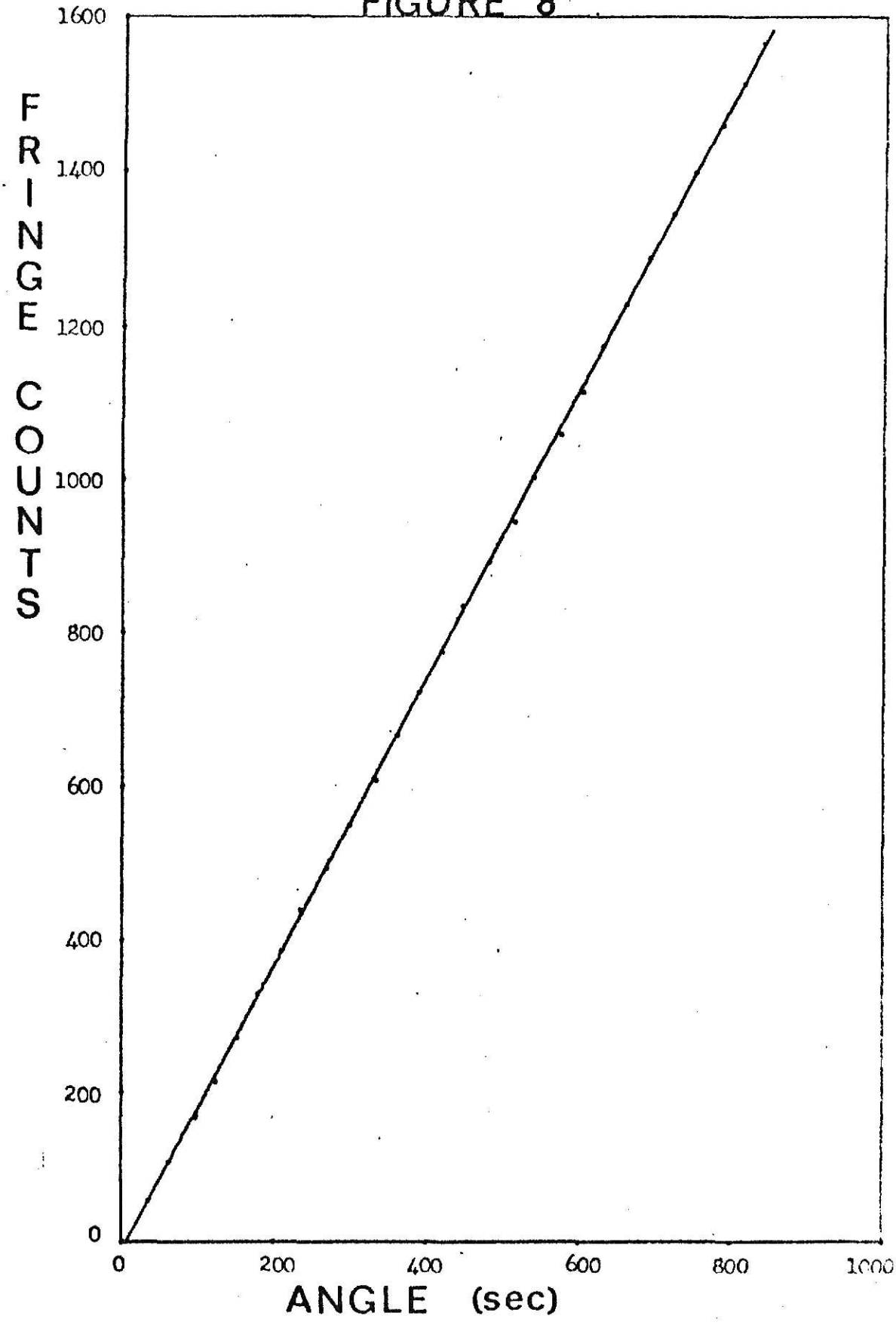
FRINGE COUNTS
1600
1400
1200
1000
800
600
400
200
0
0
200
400
600
800
1000
ANGLE (sec)

twenty aluminum sheets are shown in Fig. (9). The least squares fit to the line gave a value of 0.402 cm^{-1} with a correlation of 0.9996. Thus at the settings used during the experiment the x-ray detection and counting system were quite linear.

Now, in order to test the accuracy and use of the entire system, two calcite crystals were placed on the double crystal spectrometer, and a definite alignment procedure was followed at all times. The first crystal was set at zero angle to the beam and moved into the beam using the screw adjustment on the crystal mount until half of the beam was blocked by the crystal. Then the turntable is rotated until the planes of interest of the crystal are at the Bragg angle to the beam. Since the reflected beam must pass over the axis of the second turntable, the housing is rotated about the axis of the first turntable until the beam is cut off by a narrow pin mounted directly on the axis of the second turntable. The second crystal mount is then attached and set at zero angle to the beam. It is then positioned by the screw adjustment perpendicular to the beam, until half of the beam is blocked by the crystal. The crystal is then rotated until it is roughly at the Bragg angle by moving the mount. The counter is turned through an angle of twice the Bragg angle with respect to the original beam direction. The second crystal is then adjusted more finely by using the turntable until the Bragg peak is located. Then the adjustment screw which controls the tilt of the crystal is turned carefully until the highest intensity is reached. The second crystal is now exactly parallel to the first.

At this point two other components were added to the experimental arrangement. First, a horizontal slit system of lead was introduced between

Fig. 9: Check on the linearity of the x-ray detection system. n is the number of 1mil thick Al sheets inserted in front of the counter. The slope, 0.402/cm, should equal the linear absorption coefficient of Al. A least squares fit gave a confidence of 0.9.

FIGURE 9

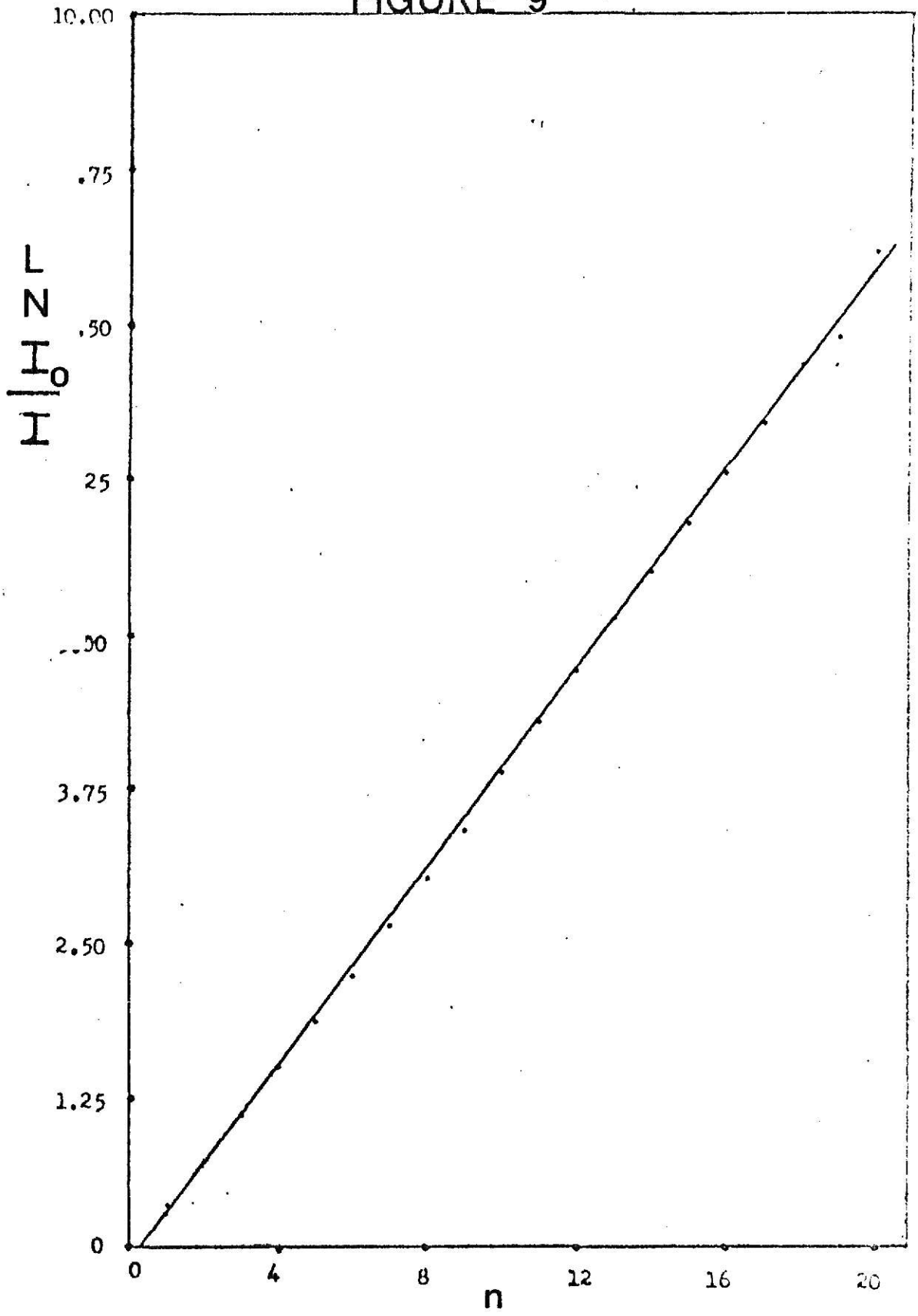

the two crystals. This consisted of two slits, the one closest to the first crystal is very narrow, about 1mm. The second is about 5mm. The purpose of the slits is to select a small horizontal slice of the beam coming from the first crystal, which limits vertical divergence, blocks straight through and scattered radiation, and limits the area of the tube target utilized. Second, a lead beam stop was placed perpendicular to the beam to block hard radiation from entering the slits at the counter. This is especially important since the counter slits must be fairly wide to insure that all of the reflected intensity from the second crystal was counted. Care must also be taken not to place the beam stop too close to the second crystal or else some scattering from the lead by the x-rays incident on the second crystal will result. This will widen the rocking curve.

The rocking curve was taken by stepping the turntable by hand approximately a second at a time and the fringe count noted. Then, at each position, x-ray counts were taken over a ten second interval. The scaler was set to count only 1/10 of the x-rays so the intensity was measured in counts per second. The background was taken to be 100 counts per second. The rocking curve plotted in Fig. (10) was taken using naturally occurring calcite from Argentina[2] and shows a full width at half maximum of 20 fringes or 10.6 arcseconds. The line through the points is a hand sketch, not a calculated fit. The theoretical value for the full width at half maximum, if Darwinian shapes (i.e. like Fig. (2)) for the reflection coefficients of the individual calcite crystal are chosen, is 10.0 arcsec. If Gaussian shapes are chosen, the full width at half maximum is 10.7 arc sec. Thus,

Fig. 10: Rocking curve of calcite taken to show the accuracy of the apparatus. The full width at half maximum obtained is 10.6 seconds of arc, which agrees with the theory if gaussian shapes are chosen for the individual reflection coefficients.

FIGURE 10

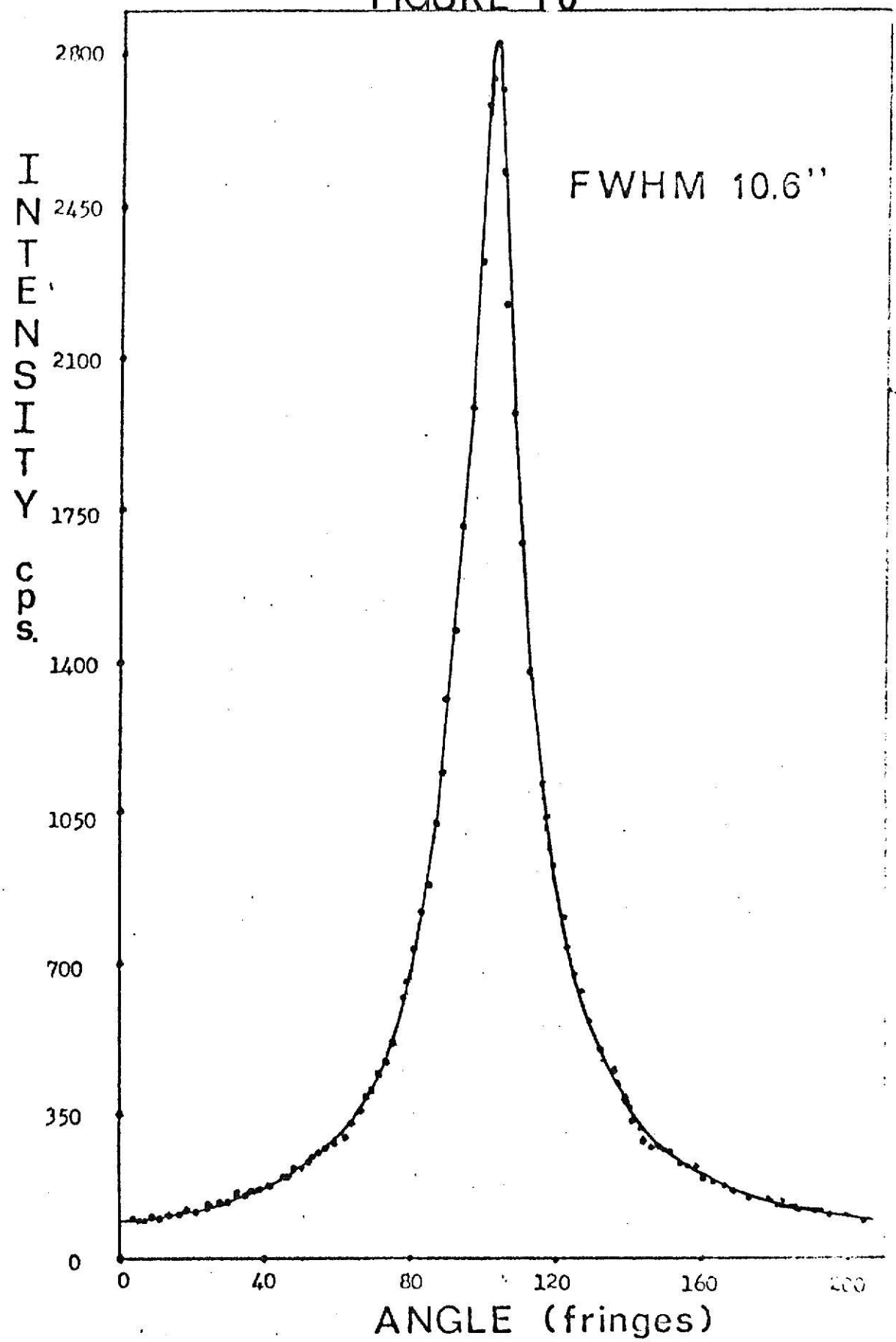
FWHM 10.6''
INTENSITY cps.
2800
2450
2100
1750
1400
1050
700
350
0
0
40
80
120
160
ANGLE (fringes)

the sensitivity and accuracy of the equipment is demonstrated upon comparison with the theoretical values.

With the accuracy and useability of the equipment established, attention was turned to examining the implanted crystals of MgO.

Sample History and Preparation

The MgO samples used were obtained from Y. Chen at Oak Ridge National Laboratory. There were two different crystals, one labeled MgO 10270 and the other labeled MgO hydrogen-free. The hydrogen free crystal had been heat treated by a process patented by Chen and according to him it is the best MgO crystal available.[3]

The samples were irradiated with Na^+ ions of 90 kev energy. The accelerator beam was approximately one and a half cm. in diameter at the sample. A rectangular mask with a slit size of 0.68cm X 0.66cm. was placed over the crystal to select the middle of the beam, thus preventing the dose from varying too greatly over the region of implant. Both sides of the crystals were implanted in this manner. The MgO 10270 crystal was mainly used in this experiment with an unimplanted MgO hydrogen-free crystal as a monochromator. The MgO 10270 was implanted to a dose of 2.5×10^{15} ions on each side. There was no other treatment given to the crystals beyond this.

The Experiment with MgO

Since there was adequate reason to believe the MgO sample was fairly perfect, the double crystal spectrometer was used. If the MgO were indeed perfect, the double crystal unit has the high resolution necessary to detect

it. The hydrogen-free crystal was used as the first crystal and the unimplanted sample of MgO 10270 as the second and rocking curves taken. Then the crystals were switched and additional curves were made. There was no difference in the curves produced, and both yielded values for the full width at half maximum of over 85 arcseconds. The theoretical width if the crystals were perfect is 13.3 arcseconds. Thus, despite the special processes used in preparing the crystals, they are still far from being perfect. The hydrogen-free crystal was returned to the first crystal position in preparation to study the implanted sample. The large widths obtained must be due to dislocations and impurities, which have always been a problem in growing MgO crystals. Luminescence studies have shown that these crystals have chromium impurity of approximately 1 part in 10^7.

The Na^+ implanted sample of MgO 10270 was mounted as crystal B and a long series of rocking curves were taken up the face of the crystal, including implanted and unimplanted regions. This was done by making the horizontal slits between crystal A and crystal B very narrow, 0.22 mm, and raising them in varying amounts of about 0.2mm. The narrow slit allowed small portions of the crystal to be sampled in a regular and repeatable way. This technique may leave something to be desired, since in doing this a different spot on the tube target is the source each time the slits were raised. Further, when the slits are positioned near the top or the bottom of the beam, the divergence is different from when the slits are in the middle. An alternate method would be to move crystal B so that different portions are in the beam. In this experiment there was no vertical adjustment on the second crystal mount requiring the crystal

to be moved by remounting each time. This would be less repeatable. The experiment for MgO was performed in the same manner as for the calcite trial discussed previously. The position at which the x-rays struck the crystal was determined by directing a laser beam through the horizontal slits and noting where it hit the crystal.

RESULTS

Of a large number of curves taken in the above manner, Fig. (11) shows four curves that depict the pattern observed in the series of trials made. The curves were started from the same angle each time. The ordinate in Fig. (10) is the x-ray intensity in counts per second, and the abscissa is the angle of rotation in fringes, where 1.877 fringes correspond to one arcsecond. The insert at the upper left in Fig. (11) is a sketch of the crystal with the implanted area shown as a cross-hatched region. The letters A, B, C, and D indicate the position on the crystal from which the respective curve was taken. Data from these four curves are summarized in Table I.

Curve A was taken in an unimplanted portion of the crystal. Its peak is located at 830 fringes, with a peak intensity of 2050 cps, and a full width at half maximum (FWHM) of 171 fringes. The asymmetry on the high angle side appears to be due to a second peak. This seems to be a characteristic of the crystal, as will be seen later.

As trials were taken moving up the crystal, a secondary peak began to appear at a lower angle than the main peak. At points just below B, it first appeared as a very broad, but slight, increase in the intensity. As the implanted region was approached, this became a more distinct peak with higher intensity. Curve B was taken just over the edge of the implanted region about 0.085 inches about the location of curve A. Here the intensity of the secondary peak has increased to 500 cps, and a FWHM of 330 fringes. It is 400 fringes below the main peak, which corresponds to 213 arcseconds,

TABLE I

	Main Peak			Secondary Peak				
	Location (fringes)	FWHM (Fringes)	Max. Int. (cps)	Location (Fringes)	FWHM (Fringes)	Seperation (Fringes)	Max. Int. (cps)	Delta a Å
Curve A	830	171	2050	-	-	-	-	-
Curve B	1060	250	1400	660	330	400	500	0.012
Curve C	840	270	1250	330	180	540	825	0.014
Curve D	1060	250	810	590	300*	470	425	0.013
				730		330	410	0.009

* FWHM for the two unresolved peaks.

Fig. 11: Four rocking curves typical of those obtained for the MgO 10270 taken at different locations on the crystal.

Legend	Position
Curve A:.....Dark blue	
Curve B:.....Light blue	0.18cm above A
Curve C:.....Red	0.33cm above B
Curve D:.....Green	0.05cm above C

FIGURE 11

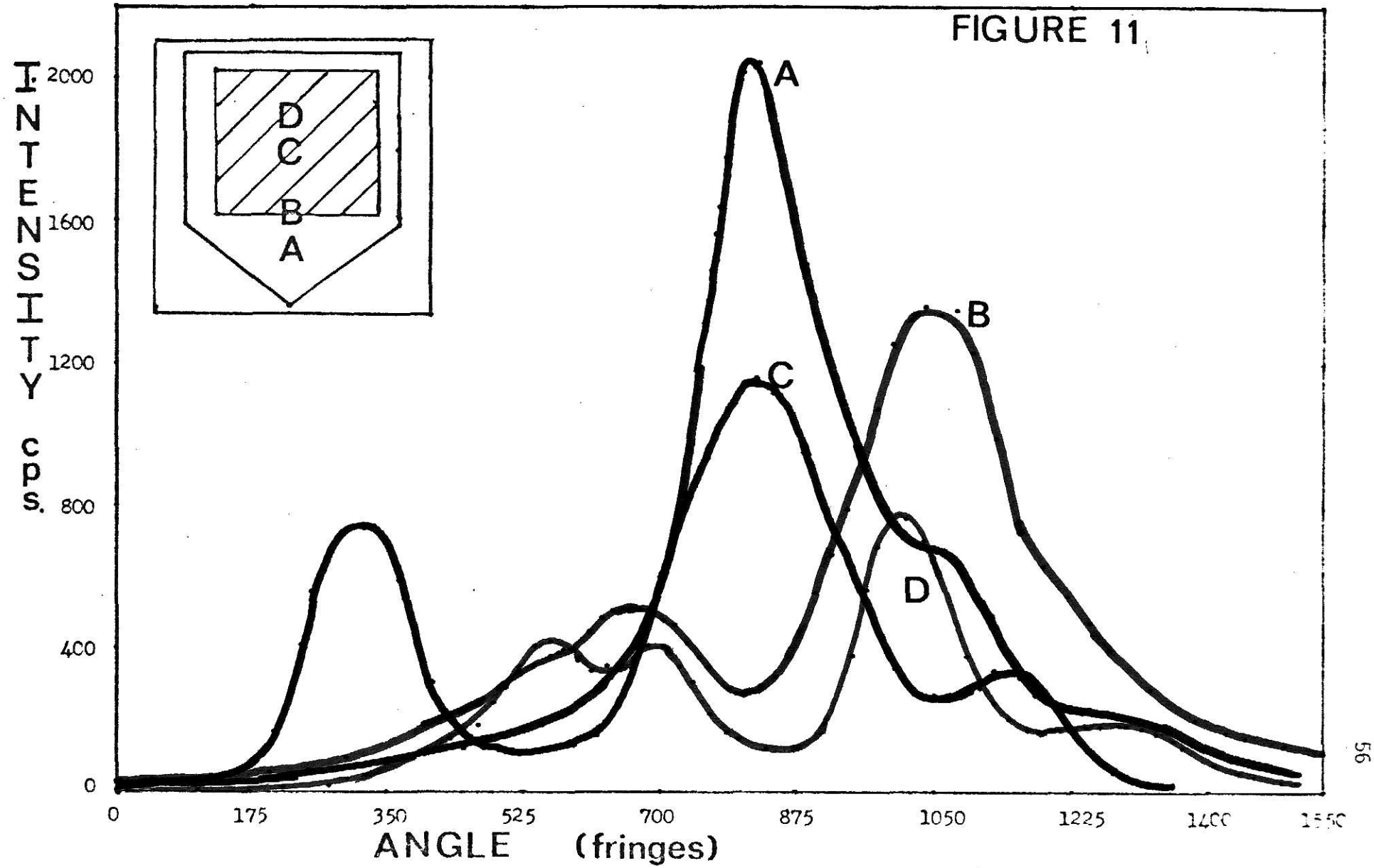
INTENSITY cps.
2000
1600
1200
800
400
0
0
175
350
525
700
875
1050
1225
1400
ANGLE (fringes)
A
B
C
D
D
C
B
A

or about 2/3 of the calculated separation made earlier in this paper. This separation was observed for other curves taken near the site of curve B. The main peak has decreased in intensity to 1400 cps and broadened to a FWHM of 250 fringes. The intensity ratio of the peaks is about 3:1. These observations were expected as discussed in the theoretical section. However, something very unexpected is shown in curve B. The main peak, which was expected to be located at the same angle as the peak in the unimplanted curve, has shifted to higher angle. This suggests that there is a region of compressed volume. This shift to higher angle was observed in other trials taken from a region near B. The size of the shift, about 230 fringes, corresponding to a .006 Å decrease in planar spacing, is similar in all of these curves. There is still some high angle asymmetry associated with the peak.

The crystal was moved so that the x-rays were incident on the very center of the implanted region. Curve C is the result of this trial. Other curves were taken near this region on the crystal, and similar results obtained. The secondary peak has increased in intensity to 825 cps and has sharpened considerably to an FWHM of 180 fringes. The peak separation in this case is 540 fringes or 288 arcseconds, which is in good agreement with the calculated value. The main peak has broadened to a FWHM of 270 fringes while the intensity has dropped to 1250 cps. The ratio of the peak intensities of the main to the secondary peak is 1.6:1. The main peak at 840 fringes has moved back to an angle very nearly that of the undamaged curve. This somewhat startling fact was reaffirmed in another curve taken a few thousandths of an inch from this curve. The high angle

asymmetry here shows up as two peaks. The fact that the secondary peak has increased sharpness and intensity suggests that there is more order in the expanded region near the center than at the edges. The return of the main peak to the unimplanted location implies that the region of the crystal under the implanted layer has the same unit cell as the unirradiated portion. The increased breadth indicates increased strain in the region.

The slits were positioned to sample a region about 0.025 in. above that for curve C. The results are shown in curve D. The secondary peak shows up as a double peak of about 410 cps intensity and a width of 300 fringes. The separation of the peaks is 475 fringes and 330 fringes on the low and high angle sides, respectively. The main peak has shifted back to higher angle by the same amount of 230 fringes. It has a FWHM of 250 fringes but the intensity has fallen markedly to 810 cps. However, the intensity is down over the entire curve. The ratio of the peak intensities is 2:1. If curve B is examined again, its secondary peak looks something like the sum of two peaks placed closer together than those in the secondary peak of curve D. This is evidenced by the large breadth and the more gradual rise to the maximum. This suggests that if one made another run near the top edge of the implant, a curve like B would result.

To summarize, then, these curves present the following facts:

(1) There is some high angle asymmetry on the main peak that appears to be characteristic of the host crystal, since as the peak moves this asymmetry moves with it.

(2) The low angle secondary peak does appear but the separation from the main peak agrees with the calculated value only in the center

of the implant. The observed value is always less than the calculated.

(3) The secondary peak narrows as one moves up to the center of the damage. Away from the center it is quite broad, apparently due to double peaks.

(4) The separation of the secondary peak from the main peak increases in moving up to the center of the implant.

(5) The ratio of the maximum intensity of the main to the secondary peak decreases as one goes from the edge to the center of the implant and rises in going towards the edge.

(6) The maximum intensity of the main peak is observed to decrease when progressing from an undamaged region to a damaged region. The FWHM increases as this is done.

(7) The main peak shifts to higher angle except at the very center of the damage. In the center, the main peak is at the same position as in the undamaged case.

DISCUSSION AND CONCLUSIONS

In order to develop a picture of what has happened to the lattice due to the implant, the implications of these data must be discussed. To begin, consider the properties exhibited by the secondary peak in Curve C. In this curve, the observed angular shift most nearly agrees with the predicted value. The discrepancy has two explanations. First, since the observed value is too small, a larger value of p' than that assumed would improve the agreement. This amounts to saying that the Na^{+} ions have a larger packing rate than the MgO, which is plausible since the ionic radius of Na^{+} is smaller than the average of the ionic radii of the Mg^{+2} and O^{-2}. A second explanation would be that the number of ions introduced, 2.5×10^{15} is somewhat high. This would of course give a value for the angular separation that is too large. In the case of Curve C, a 10% variation in the dose would bring the calculation into agreement with experiment. According to data from Dr. James MacDonald, who performed the irradiation, a fluctuation of this magnitude is possible. Thus, at least for Curve C, this simple calculation gives very good agreement with the experimental results, and the assumptions made were apparently valid ones. However, this may not be the case for other crystals and implants. Further experiment is necessary to check the formula.

In Curve B, which was taken near the edge of the implant, the angular separation is considerably different from the calculated value. This could be explained easily if the accelerator beam was non-uniform over the implant region. However, a 50% variation is required in the dose to bring the calculated value in agreement with this. A mask was used to

insure that a small region at the center of the beam was incident on the crystal. Thus, a variation of this magnitude is unlikely. The result could be explained, since the curve is taken at the edge of the implant, by the following argument: Na^+ ions incident on the crystal collide with lattice ions, generally with a non-zero impact parameter. In this collision the Na^+ ion and the recoiling lattice ion travel in a sideways direction and come to rest in a region outside the implanted volume as defined by the mask. Thus, some expansion is expected outside the region of implant giving rise to an angular shift. One, of course, would expect this to be considerably less than the expansion at the center of the implant, which is more likely due to the incident particles.

One may now ask if the change in the angular shift is continuous, and although more data are required to answer this fully, the following argument can be suggested. Curve D exhibited a double peak, each of approximately equal intensity, one giving an angular separation nearly equal to that obtained in Curve C and the other considerably less. This is the sort of result one would expect if there is a discontinuous charge in the expansion and Curve D is sampling an area almost exactly at this discontinuity. Then, Curve B is taken at a position where the smaller expansion is more predominant, but there is a contribution from the region of larger expansion which causes the long slow rise on the low angle side of its peak. Another curve, taken from a position in between C and D shows the two peaks but the contribution from the larger expansion is greater, lending further credence to this picture.

If one considers the widths and intensities of the secondary peaks for the three curves, further evidence for the above argument is seen.

Curve C exhibits a secondary peak with a FWHM slightly larger than that of the main Bragg reflection from the undamaged curve. This suggests that at least in the center of the implant, there is a high degree of ordering. The decreased intensities and greatly increased widths of the secondary peaks in B and D imply that more damage has been done to the lattice in these regions.

Thus the secondary peaks suggest a model for the implanted layer. At the center of the implant, an expansion in volume nearly equal to that predicted by a simple calculation is observed. The sharpness of the secondary peak and this agreement with the theory suggest, that at point C, the Na^+ ions are packed in between planes causing a relatively well ordered volume change.

To the sides a volume change occurs due to the sidewards motion of the recoiling knock-on atoms and incident ions. These give rise to double peaks in the secondary, depending on where the curve is taken with respect to the discontinuity.

To develop a model for the effect of the implant on the host crystal beneath the implant, the properties of the main peaks can be considered. First, the high angle assymetry must be dismissed as a property of the host crystal, since this assymetry appears in every curve.

The peaks are seen to decrease in intensity as one proceeds from the edge to the center of the damage and the FWHM increases. One expects this might be due to the strain on the crystal planes below the implant due to the swelling of the implanted layer. However, the FWHM is nearly the same for the curves A, B, and D, suggesting the strain is fairly

uniform in these regions. The increased value in C then implies a somewhat increased strain in the center of the implant where the volume change was the greatest. As one approaches the center of the damage, the intensity ratio of the main to the secondary peak lowers, and then increases in passing through the center. This means that as the secondary is sharpening up, the main peak is becoming wider and lower. It should be pointed out that although the low intensity of D is puzzling, its intensity ratios and widths fit the proposed picture very well.

Perhaps the most startling fact uncovered in the experiment is the high angle shift exhibited by the main peak. A shift to higher angle implies a decrease in volume and thus a contraction of the lattice, and a mechanism for this process is sought. One may first conjecture that the implant has pushed the planes below it together until a slightly smaller planar spacing occurred. However, this would not fit with the curves taken at the middle of the implant, which shows the original spacing. The contracted region must be to the sides of the implant, and the planes must appear "pinched" together in this region. To this author's knowledge, this is the first time such a phenomenon has been reported. The size of the shift indicated a new lattice parameter of 4.2066 Å. The exact mechanism for this is somewhat puzzling and certanly bears further examination. However, a tentative suggestion can be offered. Since the phenomenon requires that the planes be "pinched" on the sides of the implant and unaffected in the center, the planes must be bent in a convex fashion. Kishino and Noda[8] observed the convex bending of Silicon wafers that had been implanted, so there is some precedence for this process. The MgO

crystals used were too thick for the entire crystal to exhibit bending, as was observed by Kishino and Noda. The modification to the crystals used here would be that only the crystal planes near the implanted layer would be bent. Those deeper down in the crystal remain straight thus creating the "pinched" region. Kishino and Noda found that convex bending occurred upon implantation regardless of the size of the projectile. Upon anneal however, if the projectile was smaller than the atoms the host wafer bent concavely. One could then test the proposed mechanism in the case of MgO by annealing and taking additional rocking curves. It would also be interesting to study this in other host crystals and implants. That the shift occurs, at least in MgO, is well documented in this study with many curves taken to confirm it. Preliminary studies on the MgO hydrogen free crystal again reveal a high angle shift of about the same magnitude. Thus this effect appears in another MgO crystal, which has been treated by a somewhat different process. This crystal has been heated to very high temperature to anneal out grown-in dislocations. It seems that the high angle shift is not due to some defect or property peculiar to the MgO 10270 crystal.

Whether or not it is peculiar to MgO, details on the mechanism and what factors affect the size of the shift, remain for further study.

SUMMARY

While the study has raised many questions, a model of the implanted crystal can be concluded. The implanted layer exhibits an expanded volume. The magnitude of the expansion can be calculated using a simple-minded formula by making the assumption that the incident particles pack at the same rate as the lattice atoms, and all the incident particles come to rest as interstitials creating negligible vacancies. For this sample, the agreement was quite good in the very center of the implant but was rather poor at the sides. This implies that at the center there is a region of increased volume, while to the sides, there is a less expanded volume. This region of lesser expansion is due not to a fluctuation in dose, but due to the sidewards movement of the recoiling ions. Whether or not this volume change is a continuous one, is not quite clear but it seems that it is neither very smooth nor very abrupt. The planes beneath the implant are strained or suffer from some types of defects as evidenced by the increased widths. These planes also seem to be bent in a convex fashion giving rise to a decrease in volume near the sides of the implant.

REFERENCES

1. K. J. Bachmann, T. O. Baldwin, F. W. Young, Journal of Applied Physics, 41, 4783 (1970).

2. J. A. Bearden, private communication.

3. Y. Chen, private communication.

4. A. H. Compton and S. K. Allison, X-Rays in Theory and Experiment (D. VanNostrand Co., New York, 1935), Second Edition, p. 709.

5. J. R. Crawford and R. D. Dragsdorf, Journal of Applied Physics 44, 385 (1973).

6. P. H. Dederichs, Physical Review B 4, 1041 (1970).

7. W. S. Johnson and J. F. Gibbons, Projected Range Statistics in Semiconductors (Stanford University Bookstore, Palo Alto, 1970), Appendix.

8. S. Kishine and A. Noda, Journal of the Japan Society of Applied Physics 42, 118 (1973).

9. M. A. Krivoglaz and K. P. Ryaboshapka, Fiz. Metal. Metalloved. 15, 18 (1963).

10. R. W. James, The Optical Principles of the Diffraction of X-Rays (G. Bell and Sons, Ltd., London, 1948), p. 52, 304.

11. J. Linhard, M. Scharff, H. E. Schiott, Mat. Fys. Medd. Dan. Vid. Selsk. 33, (1963).

12. J. G. Marzolf, The Review of Scientific Instruments 35, 1212 (1964).

13. J. R. Patel, R. S. Wagner, S. Moss, Acta Metallurgica 10, 759 (1962).

14. B. Petry and M. Pluchery, C. R. Acad. Sc. Paris 272 B, 240 (1962).

15. J. E. Thomas, T. O. Baldwin, P. H. Dederichs, Physical Review B 3, 1167 (1971).

16. B. E. Warren, X-Ray Diffraction (Addison-Wesley Publishing Co., Reading, Mass., 1969), p. 315.

ACKNOWLEDGEMENTS

The author would like to extend his sincere thanks to Dr. R. D. Dragsdorf for his guidance and pedagogy, which have made this research pleasureable as well as a tremendous learning experience.

Tom Lehman, who constructed the interferometer and fringe counting circuit, and Dr. James MacDonald, who performed the irradiations, must also be acknowledged for their contribution to this research.

The author is also very grateful to M. D. Shaw for his suggestions on perfecting the electronics of the fringe counter, and to Dr. A. Compaan for some very helpful comments on the optics of the interferometer.

Finally, to Ms. Wanda de Workman, the author is indebted for her assistance in the lab and discussions on the results, and for her support during this entire program of research. She has made the task even more rewarding.

AN X-RAY DOUBLE CRYSTAL SPECTROMETER STUDY OF SINGLY-IONIZED SODIUM-IMPLANTED MAGNESIUM OXIDE

by

RICKY LYNN WORKMAN

B.S., Mississippi State University, 1972

AN ABSTRACT OF A MASTER'S THESIS

submitted in partial fulfillment of the
requirements for the degree

MASTER OF SCIENCE

Department of Physics

KANSAS STATE UNIVERSITY
Manhattan, Kansas

1974

This research has led to two main accomplishments. First, a double crystal spectrometer and angle measuring system have been developed and shown to be operating at a level of precision adequate for this research study. This process consisted mainly of perfecting the angle measuring interferometer and electronic counting device, although the use of this technique required some modifications to the double crystal unit itself. As a demonstration of the capability of the apparatus, rocking curves of calcite were taken and the full width at half maximum were compared to the theoretical value calculated for this crystal.

In addition Na^+-implanted samples of MgO were studied and a simple-minded theoretical calculation was developed which, at least partially, explained the results. The implantation produced secondary peaks in the rocking curve from the expanded volume of the implanted region of the crystal. The main Bragg reflection was observed to shift to a higher angle suggesting a region of compressed volume below the implanted layer. This is attributed to convex bending of the lattice planes directly underneath the implant, which creates a pinched region. Such a phenomenon has not been reported before, however this experiment produced considerable evidence that the compression occurs. Further study is necessary to understand fully the mechanism involved.